PERGAMON

Deep-Sea Research II 49 (2002) 1573–1596

DEEP-SEA RESEARCH
PART II

www.elsevier.com/locate/dsr2

# Indian Ocean dipole mode events in an ocean general circulation model

P.N. Vinayachandran[a,*], Satoshi Iizuka[b,1], Toshio Yamagata[c,1]

[a] *Centre for Atmospheric and Oceanic Sciences, Indian Institute of Science, Bangalore 560 012, India*
[b] *National Research Institute for Earth Science and Disaster Prevention, Tennodai 3-1, Tsukuba, Ibaraki 305-0006, Japan*
[c] *Department of Earth and Planetary Physics, Graduate School of Science, The University of Tokyo, Tokyo 113-0033, Japan*

Accepted 27 September 2001

**Abstract**

The evolution of the dipole mode (DM) events in the Indian Ocean is examined using an ocean model that is driven by the NCEP fluxes for the period 1975–1998. The positive DM events during 1997, 1994 and 1982 and negative DM events during 1996 and 1984–1985 are captured by the model and it reproduces both the surface and subsurface features associated with these events. In its positive phase, the DM is characterized by warmer than normal SST in the western Indian Ocean and cooler than normal SST in the eastern Indian Ocean. The DM events are accompanied by easterly wind anomalies along the equatorial Indian Ocean and upwelling-favorable alongshore wind anomalies along the coast of Sumatra. The Wyrtki jets are weak during positive DM events, and the thermocline is shallower than normal in the eastern Indian Ocean and deeper in the west. This anomaly pattern reverses during negative DM events.

During the positive phase of the DM easterly wind anomalies excite an upwelling equatorial Kelvin wave. This Kelvin wave reflects from the eastern boundary as an upwelling Rossby wave which propagates westward across the equatorial Indian Ocean. The anomalies in the eastern Indian Ocean weaken after the Rossby wave passes. A similar process excites a downwelling Rossby wave during the negative phase. This Rossby wave is much weaker but wind forcing in the central equatorial Indian Ocean amplifies the downwelling and increases its westward phase speed. This Rossby wave initiates the deepening of the thermocline in the western Indian Ocean during the following positive phase of the DM. Rossby wave generated in the southern tropical Indian Ocean by Ekman pumping contributes to this warming. Concurrently, the temperature equation of the model shows upwelling and downwelling to be the most important mechanism during both positive events of 1994 and 1997. 

## 1. Introduction

The El Niño Southern Oscillation (ENSO) has been well recognized as the dominant signal of the interannual variability in the Pacific Ocean (Philander, 1990). Several investigations suggest that ENSO-related warming takes place in the Indian Ocean as well (Tourre and White, 1997; Chambers et al., 1999 and references therein). In contrast,

*Corresponding author. Tel.: +91-80-309-2505; fax: +91-80-360-0865.

*E-mail address:* vinay@caos.iisc.ernet.in (P.N. Vinayachandran).

[1] Also at Institute for Global Change Research, Frontier Research System for Global Change, Tokyo, Japan.

0967-0645/02/$ - see front matter 
PII: S0967-0645(01)00157-6

Saji et al. (1999, hereafter referred to as SGVY) and Webster et al. (1999) have recently demonstrated that the anomalous conditions that occurred in the Indian Ocean during certain years are independent of ENSO. In particular, SGVY discovered that a dipole mode (DM) exists in the Indian Ocean characterized by warm sea-surface temperature (SST) anomalies in the western Indian Ocean and cold SST anomalies in the eastern Indian Ocean in its positive phase (Fig. 1, left panels). The SST anomalies are accompanied by easterly wind anomalies in the equatorial Indian Ocean and upwelling-favorable alongshore wind anomalies off Sumatra. The sea-surface height remained lower than normal in the east and higher in the west (Chambers et al., 1999). This pattern reverses during the negative phase of the DM (Fig. 1, right panels), which is much weaker than the positive phase. The DM is phase-locked to the seasonal cycle in the Indian Ocean, and the peak strength of the anomalies generally occur during boreal fall. Both atmosphere and ocean are affected by the DM. There are indications that droughts in Indonesia, rainfall over India and Australia and the east African rainfall are influenced by the DM (see SGVY, Webster et al., 1999 and references therein). In the ocean, the DM event during 1997–1998 caused a phytoplankton bloom in the eastern equatorial Indian Ocean off the coast of Sumatra (Murtugudde et al., 1999).

The strongest of the known positive DM events occurred during 1997–1998, coinciding with the most intense ENSO in the recent decades. The SST in the eastern Indian Ocean was cooler by more than 2°C and the western Indian Ocean was warmer by more than 2°C (Yu and Reinecker, 1999; Webster et al., 1999). The east–west contrast in SST in turn maintained the wind anomalies for a longer period by coupled ocean–atmosphere interactions (SGVY; Webster et al., 1999). The wind anomalies alters the thermal structure of the equatorial Indian Ocean from its normal east–west orientation. Eastward Kelvin waves, produced by anomalous easterlies, lift the thermocline in the eastern Indian Ocean, and alongshore winds off Sumatra enhances the cooling in the eastern Indian Ocean (Murtugudde et al., 2000). They also found that warming in the western Indian Ocean was caused by weak southwest monsoon winds and meridional advection and was sustained until early 1998 by a downwelling Rossby wave. The southeasterly trades in the southern tropical Indian Ocean were shifted towards the equator, and the consequent reduction in latent heat flux was found to be responsible for the warming in the southwestern part of the Indian Ocean (Yu and Reinecker, 2000). Analysis of sea-surface height (SSH) anomalies from TOPEX/Poseidon suggests that westward propagating Rossby waves forced by wind anomalies also cause warming in this region (Chambers et al., 1999).

A positive DM event similar to the above but weaker in magnitude occurred during 1994 (Vinayachandran et al., 1999b). Cold SST anomalies exceeding 1°C were observed in the eastern Indian Ocean. The winds in the equatorial Indian Ocean were rather unusual during 1994; instead of being westerlies during spring and fall, they were easterlies. Consequently, the eastward (Wyrtki, 1973) jets in the equatorial Indian Ocean were very weak (Reppin et al., 1999). This caused the mixed layer and thermocline to be abnormally thin and shallow in the eastern equatorial Indian Ocean. The winds also had a strong alongshore component off Sumatra, favorable for upwelling. The cold SST anomalies suppressed convection over the eastern Indian Ocean (Behera et al., 1999). Other significant positive DM events since 1950 occurred during 1961, 1967, 1972, and 1982 (SGVY).

Previous studies focussed on the events of 1994 and 1997 that were positive DM events. Though observations indicate that events of the opposite sign do occur (SGVY), very little is known about the negative phase. Knowledge of the sequence of events in both phases may hold a key to understand the coupled mode in the Indian Ocean during DM events. In a previous study the simulation of the DM events in a coupled model was presented (Iizuka et al., 2000). In this paper, we examine the evolution of the DM events using an ocean general circulation forced by NCEP reanalysis (Kalnay et al., 1996) fluxes for more than 25 years. The objective of this paper is to present the seasonal evolution of the DM events in the Indian Ocean by analyzing both surface and

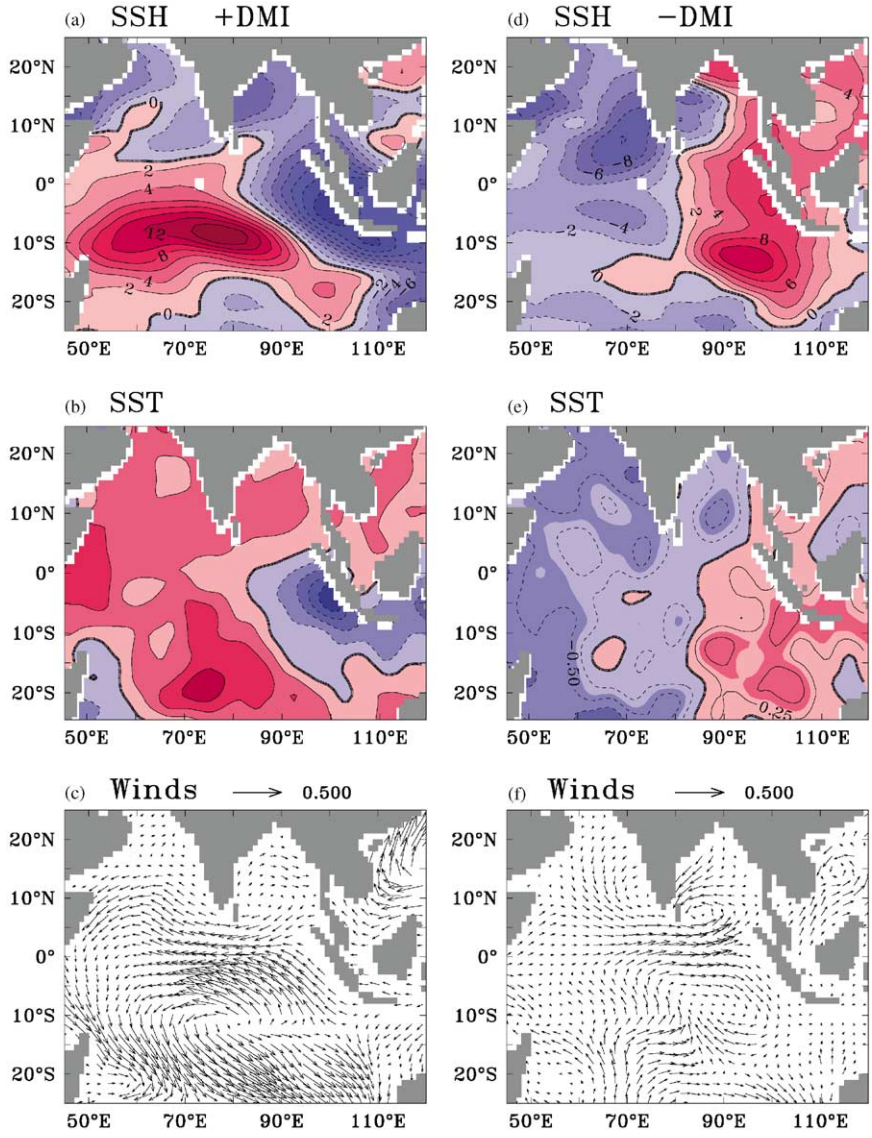


Fig. 1. Observed September–November composite anomalies, during positive dipole mode events (left panels) and negative dipole mode events (right panels). 1997, 1994 and 1982 are chosen for positive dipole mode events and 1996, 1993 and 1984 are chosen for negative dipole mode events in order to make the composites (see Fig. 2). Positive SSH and SST anomalies are shown in shades of red and negative anomalies in shades of blue.

surface signatures from the model simulation and by comparing them with observations. We also examine the role of Rossby waves as a dynamical process responsible for setting up the observed anomalies in the ocean model.

## 2. The model

The ocean model is based on the well-known GFDL Modular Ocean Model (Pacanowski, 1996). The model domain covers the global ocean

except the Mediterranean Sea and the region to the north of 80°N. The model topography is derived from the ETOPO5 data set. The horizontal resolution is 1.125° in longitude and 0.5625° in latitude, which is chosen to facilitate coupling with T106 atmospheric model (Matsuura et al., 1999). There are 37 levels in the vertical of which 25 are in the upper 400 m, making it ideal for investigating the upper layer of the ocean. The coefficient of vertical mixing depends on the Richardson number, as in the parameterization proposed by Pacanowski and Philander (1981). The biharmonic scheme is used for horizontal mixing, in which coefficients of both horizontal eddy viscosity and diffusivity are $5 \times 10^{20}$ cm$^4$ s$^{-1}$. Since no sea-ice model is included, temperature and salinity in the region poleward of 60°S and 60°N are restored to their climatological values Levitus, 1982). The external mode is solved using the method developed by Dukowicz and Smith (1994), and for convection the scheme introduced by Marotzke (1991) is used.

The model was started from a state of rest and annual mean climatological temperature and salinity (Levitus, 1982). First, the model was spun up for 20 years using climatological wind stress (Hellerman and Rosenstein, 1983). The surface temperature and salinity were restored to climatological (Levitus, 1982) monthly mean data using a Newtonian damping time scale of 15 days. Then the model was integrated for 26 years from 1973 to 1998 using the surface fluxes calculated from the NCEP/NCAR reanalysis. Wind stress and heat fluxes are calculated using the bulk formulation (see Appendix A). The penetration of solar radiation is parameterized according to the formula given by Paulson and Simpson (1977). Surface salinity is relaxed to the climatological monthly mean salinity with a time scale of 15 days. Monthly mean outputs from January 1975 to September 1998 are used in the present analysis.

Kawamura et al. (2001) used the model output to examine the role of oceans in the monsoon-ENSO coupling. They found that the model reproduces the observed composite SST anomalies of weak and strong monsoons reasonably well during spring and summer. Iizuka et al. (2000) coupled this OGCM with an atmospheric model and examined the DM simulated by that coupled model and found that the coupled model accurately reproduces the spatial pattern of the dipole mode.

## 3. The model dipole mode

In order to validate the model output we use SST from GISST2.3b data set (Rayner et al., 1996), gridded SSH anomalies measured by the altimeter on board TOPEX/Poseidon (Tapley et al., 1994; Chambers et al., 1997), and subsurface temperature from the Joint Environmental Data Analysis (JEDA) Center at the Scripps Institution of Oceanography. In the latter data set temperature observed in the upper 400 m of the global oceans are quality-controlled and the temperature anomalies are mapped into 2° latitude by 5° longitude and monthly grids using an objective procedure (White et al., 1988; (jedac.ucsd.edu). Majority of these observations in the Indian Ocean are made using expendable bathythermographs (XBT) and are concentrated along major shipping tracks (Meyers and Pigot, 2000).

### 3.1. Dipole mode index

The dipole mode index (DMI) is defined as the difference in the SST anomalies between the western and eastern parts of the Indian Ocean (SGVY). The SST anomalies are averaged over 50°E–70°E, 10°S–10°N for the western Indian Ocean and over 90°E–110°E; 10°S–0° for the eastern Indian Ocean. Fig. 2 compares the DMI from the model with that of the observations. Similar index derived from the SSH anomalies also are shown. During the 1975–1998 period three significant DM events occurred during 1982, 1994 and 1997 (SGVY). These three are the prominent events in the model results as well. The model DMI agrees very well with the observed index during 1994 and 1997, but the observed signal is weaker than the model DMI during 1982. The time series also shows that negative DM events of significant magnitude (DMI exceeding one standard deviation) do occur. Among these the most significant is the event during 1996 where both

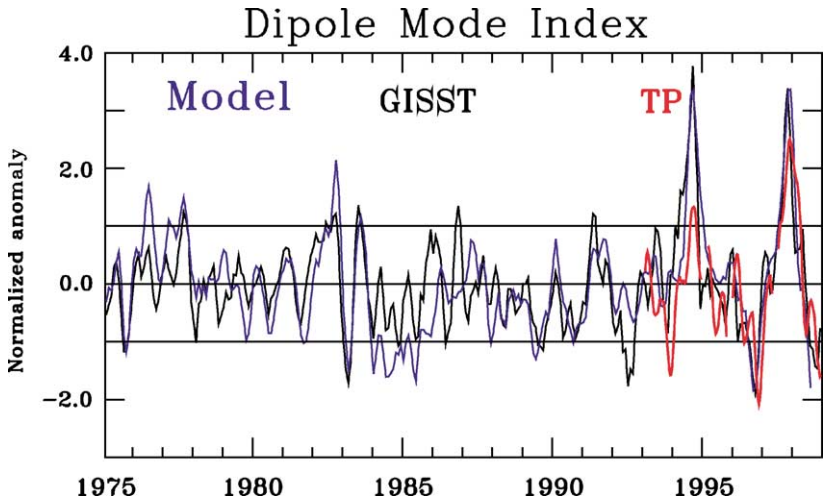


Fig. 2. Dipole mode index for the period 1975–1998. Blue line corresponds to model DMI and black line corresponds to DMI calculated from GISST2.3b. The red curve is a similar index derived from SSH anomalies. The indices are normalized by their respective standard deviations and smoothed by 5-month running mean. Standard deviation of the observed DMI time series is 0.38°C, that of the model DMI is 0.53°C and that from the SSH is 10.14 cm.

model and observations show large negative values. While the qualitative agreement between the observed and model indices is generally good for the entire period considered, there are periods when the differences are large. The most prominent difference is during 1984–1985 and 1992; both observations and model show negative DMI, but the amplitude is larger in the model. In the rest of the paper we shall focus on the two positive DM events during 1994 and 1997 and on the negative DM events during 1996 as they are best captured by the model.

### 3.2. SST anomalies

Fig. 3 compares the SST anomalies during the peak phase of the DM events. The observed pattern of the anomalies with cold SST anomalies off the coast of Sumatra and warm western Indian Ocean during positive DM is well simulated by the model. The magnitude of the anomalies exceed 2.0°C near the coast of Sumatra in both data and model (Fig. 3, upper panels). The SST anomalies extend in a zonal band along the equator farther westward in the model than in the observations. During the 1994 DM event maximum value of the cold SST anomaly is 2.0°C in the observations but 1.5°C in the model (Fig. 3 middle panels). The warm anomalies in the western Indian Ocean are larger in the observations by 0.5°C than in the model. During the negative DM of 1996 the warm anomalies exceeding 1.5°C have their maximum at about 10°S, 100°E. The cold anomalies in 1996 have their maximum value in the west in the Arabian Sea. Observations show warm anomalies only in the southeastern part of the ocean, but in the model they spread farther westward than in the observations (Fig. 3 lower panels). The difference between the observed and model SST anomalies in the western Indian Ocean is mainly due to the inaccuracies of the NCEP fluxes used for forcing the model (Yu and Reinecker, 2000). Murtugudde et al. (2000) noted that the SST anomalies during 1997–1998 is sensitive to the atmospheric fluxes used for forcing the model. Although the magnitudes of the simulated SST anomalies differ from observations by about 0.5°C, the model simulates the patterns of SST anomaly during both phases of the DM reasonably well, suggesting that model results are suitable to investigate the physics of the DM events.

### 3.3. Mixed layer and thermocline

The mixed-layer depths (MLD) obtained from the JEDAC subsurface temperature data set are

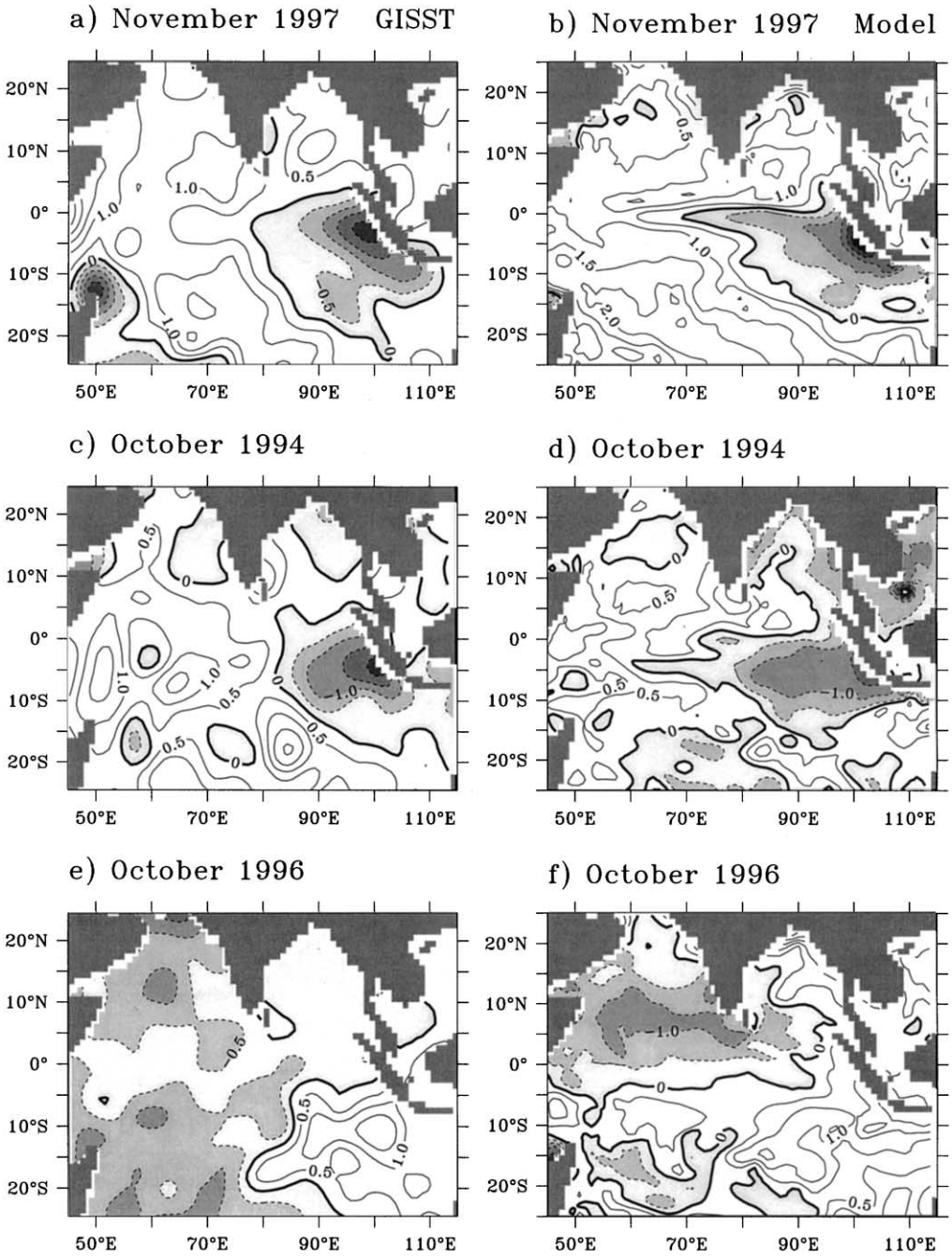


Fig. 3. Comparison of the SST anomaly simulated by the model (right panels) with observations from GISST2.3b (left panels) during the dipole mode events of 1997, 1994 and 1996. Contour interval is 0.5°C.

compared with the MLD calculated from the model temperature field in Fig. 4. After examining the sampling frequency along the XBT lines (Meyers and Pigot, 2000) the climatology is defined for the period 1986–1998 and the anomalies are calculated with respect to this period.

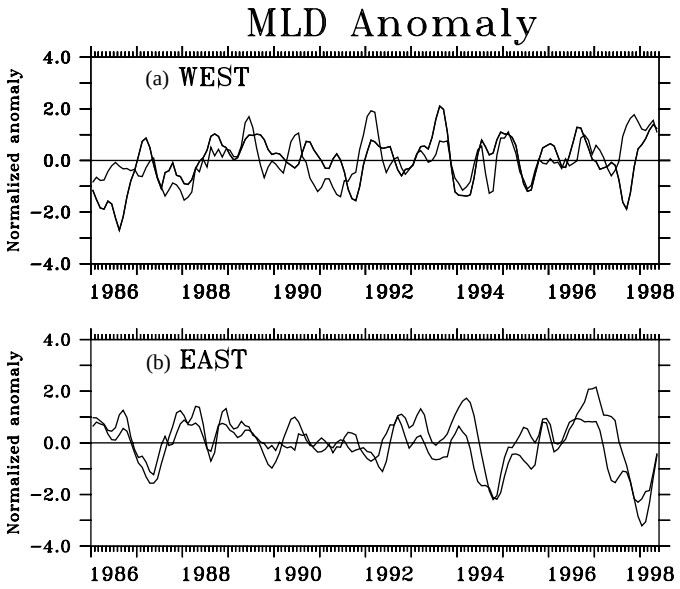


Fig. 4. Comparison of the depth of the mixed layer (MLD) in the model with observations. Anomalies of MLD with respect to 1986–1998 are shown for (a) western Indian Ocean and (b) eastern Indian Ocean (see text). The anomalies are normalized by their standard deviation and smoothed by 3-month running mean. Mixed-layer depth is defined as the depth at which the temperature is lowered by 1°C from its value at the surface or in the first model layer. Thick and thin lines correspond to observations and model, respectively.

Similar anomalies are calculated from the model result for comparison. For the western and eastern Indian Ocean regions average of the anomalies are calculated over 50°E–70°E, 10°S–10°N and 90°E–110°E, 10°S–5°N, respectively.

Fig. 4a compares the simulated mixed-layer-depth anomaly with observations in the western Indian Ocean and Fig. 4b presents a similar plot for the eastern Indian Ocean. The simulated mixed layer in the eastern Indian Ocean compares well with the observations (Fig. 4b). The shallowing of the mixed layer during 1997 and 1994 is very similar in both observations and model. Both shows a deeper mixed layer anomaly during 1996, although the deepening is overestimated in the model. In the western Indian Ocean (Fig. 4a) the model results show a deeper than normal mixed layer during the fall of 1997, but the observations indicate a shallow mixed layer followed by deepening a few months later. During 1994, the observations show a deeper mixed layer during summer and fall, but in the model results this deepening is interrupted by a distinct shallowing during summer. The difference between the model and observations in the western Indian Ocean is partly due to the model bias. Equatorial upwelling in the model is rather strong, and it penetrates far into the west (see also Fig. 3). The differences in the west is also due to the inaccuracies of the NCEP fluxes in the western Indian Ocean (Yu and Reinecker, 2000; Murtugudde et al., 2000).

The depth of the 20°C isotherm (D20) has been chosen as a proxy for the thermocline. Comparison of the simulated D20 with the observed D20 for the western and eastern Indian Ocean is shown in Fig. 5. The observed D20 anomalies offer a better comparison with the model results than the MLD anomalies because D20 reflects ocean dynamics rather than thermodynamics. During the positive DM events of 1994 and 1997 the thermocline rises in the eastern equatorial Indian Ocean (Fig. 5b), while it sinks in the western Indian Ocean (Fig. 5a). The thermocline deepens in the east during 1996 corresponding to a negative DM event. In the west, model result shows a shallowing of the thermocline but in the observations this shallowing is rather weak.

In short, both observations and model show that the positive DM events are associated with a shallowing of the thermocline in the eastern Indian

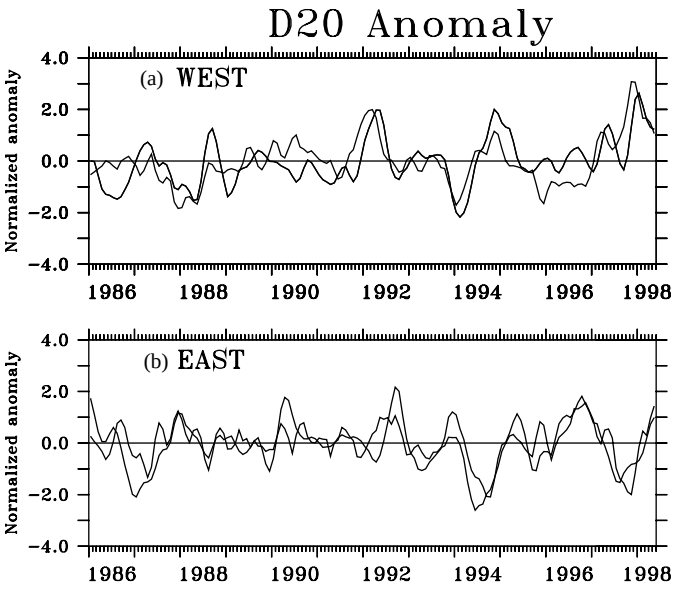


Fig. 5. Comparison of the depth of the 20°C isotherm (D20) in the model with observations. Anomalies of D20 with respect to 1986–1998 are shown for (a) western Indian Ocean and (b) eastern Indian Ocean (see text). The anomalies are normalized by their respective standard deviations and smoothed by 3-month running mean. Thick and thin lines correspond to observations and model, respectively.

Ocean and a deepening in the west. During a negative DM event the opposite pattern prevails. The sea-saw in thermocline between east and west is elucidated in Fig. 5a and b. In the eastern Indian Ocean the shallow thermocline corresponds to a thinner mixed layer and vice versa. Such a synchronous variation is not seen in the west. The observed mixed layer appears to be deeper during 1994 and 1996 but shallower during 1997. The reason for this is not clear. However, it appears that, the MLD variation in the eastern Indian Ocean is controlled by ocean dynamics, but in the west it is additionally modulated by air–sea interaction. This issue is examined later in this paper.

## 4. Evolution of the dipole mode events

Both surface and subsurface anomalies in the observations and model demonstrate that positive DM events occurred during 1997 and 1994 and a negative DM during 1996. In this section, we present the seasonal evolution of these events in the model focussing on these three events.

### *4.1. Positive phase: 1997 and 1994*

The southeasterly trades in the southern tropical Indian Ocean shift equatorward during positive DM events (Yu and Reinecker, 2000). These anomalies then move equatorward and westward during summer and fall and weaken during winter (Fig. 6). The equatorial region presents easterly wind anomalies and off Sumatra there are alongshore wind anomalies. The southwest monsoon winds during summer are weak along the coast of Sumatra but stronger in the Arabian Sea and the Bay of Bengal. The main difference between 1994 and 1997 is in the timing in the appearance of the southeasterly winds anomalies. These anomalies appear few months earlier during 1994 than in 1997. The easterly wind anomalies along the equator persist through early 1998, whereas they decay considerably during early 1995.

Cold SST anomalies off Sumatra appeared first in the model results during summer of 1997 (Fig. 7, left panels), reached their peak during fall, and disappeared by early next spring. After forming off the coast of Sumatra, the anomalies

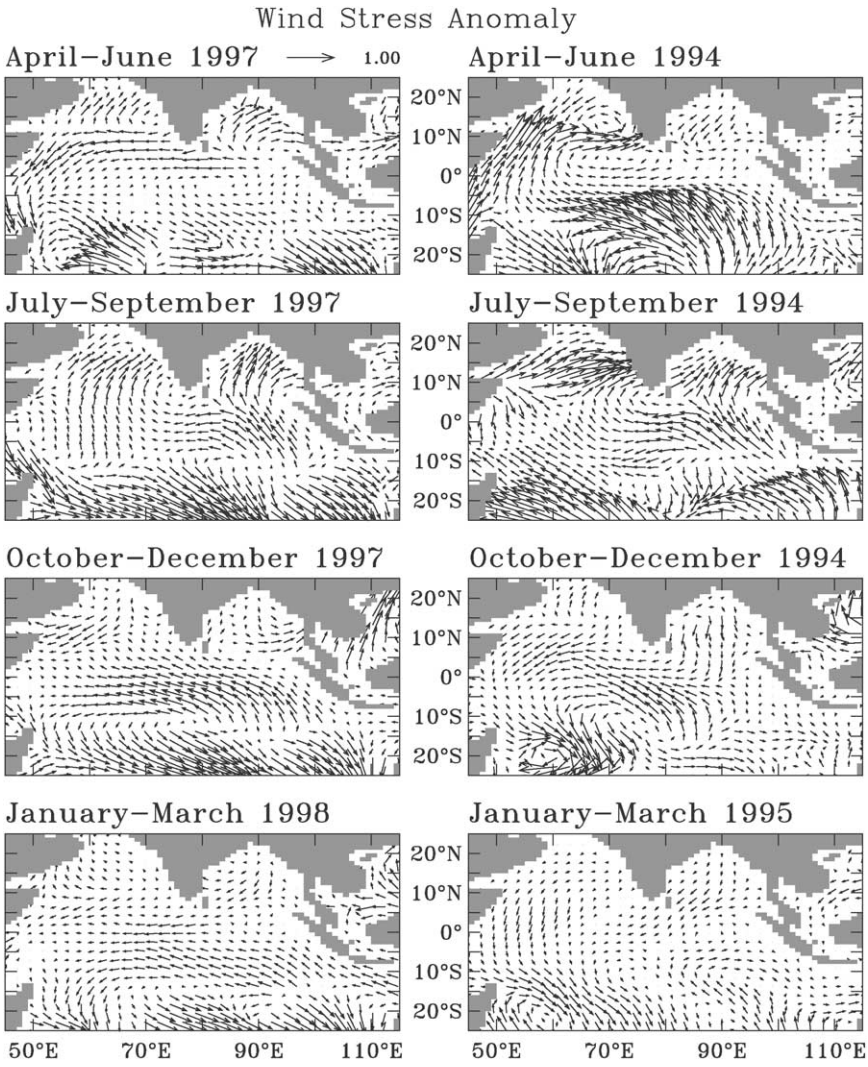


Fig. 6. Seasonal evolution of the anomalies of wind stress (dyne $cm^{-2}$) during the positive DM events of 1997 (left panels) and 1994 (right panels).

spread westward and along the equator. During 1994, weak SST anomalies (Fig. 7, right panels) appeared along the southern part of Sumatra during spring. The cold SST anomalies reached their peak during summer compared to 1997 when the peak was during fall. Warm SST anomalies in the western part of the Indian Ocean in 1994 appeared later than during 1997 due to the strong southwesterly winds during the early stages of summer monsoon of 1994 (compare top panels of Fig. 6). This reduced the east–west contrast and hence the DMI during 1994. During its decay phase, the Indian Ocean showed a basin-wide warming during early 1998 but cooling during 1995 (Fig. 7 bottom panels).

The subsurface anomalies (Fig. 8a, b) caused by the upward movement of the isotherms are much larger than their surface counterpart; the magnitude of the anomalies is as large as 6°C at a depth of about 100 m. The dipole pattern is present

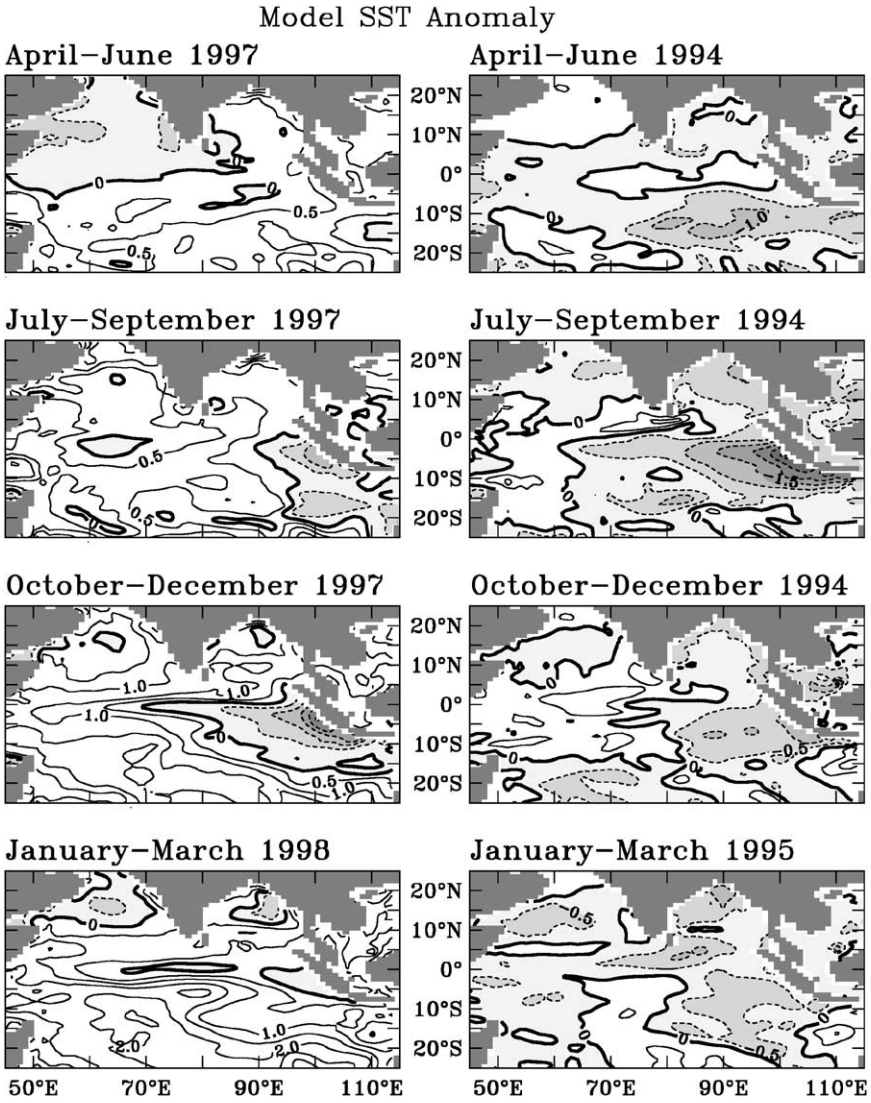


Fig. 7. Seasonal evolution of the anomalies of model SST during the positive DM events of 1997 (left panels) and 1994 (right panels). Contour interval is 0.5°C. Negative anomalies are shaded.

down to a depth of about 200 m. This verifies the importance of ocean dynamics in the DM events.

The negative anomalies in MLD during 1994 also appeared in the east during spring compared to summer in 1997. This was accompanied by a shoaling of the thermocline, with maxima on either side of the equator (Fig. 9), which is well supported by observations (Fig. 10). The negative anomalies moved westward as an equatorial Rossby wave as can be seen from the D20 anomalies (Fig. 9). Outside the band of negative anomalies the thermocline showed deepening with maximum at about 10°S during fall and winter. In the west, the deepening of the thermocline began during summer and reached its peak during fall.

In the tropics, the oscillations of the thermocline are generally reflected in the SSH variations. Therefore, we have presented the SSH anomalies

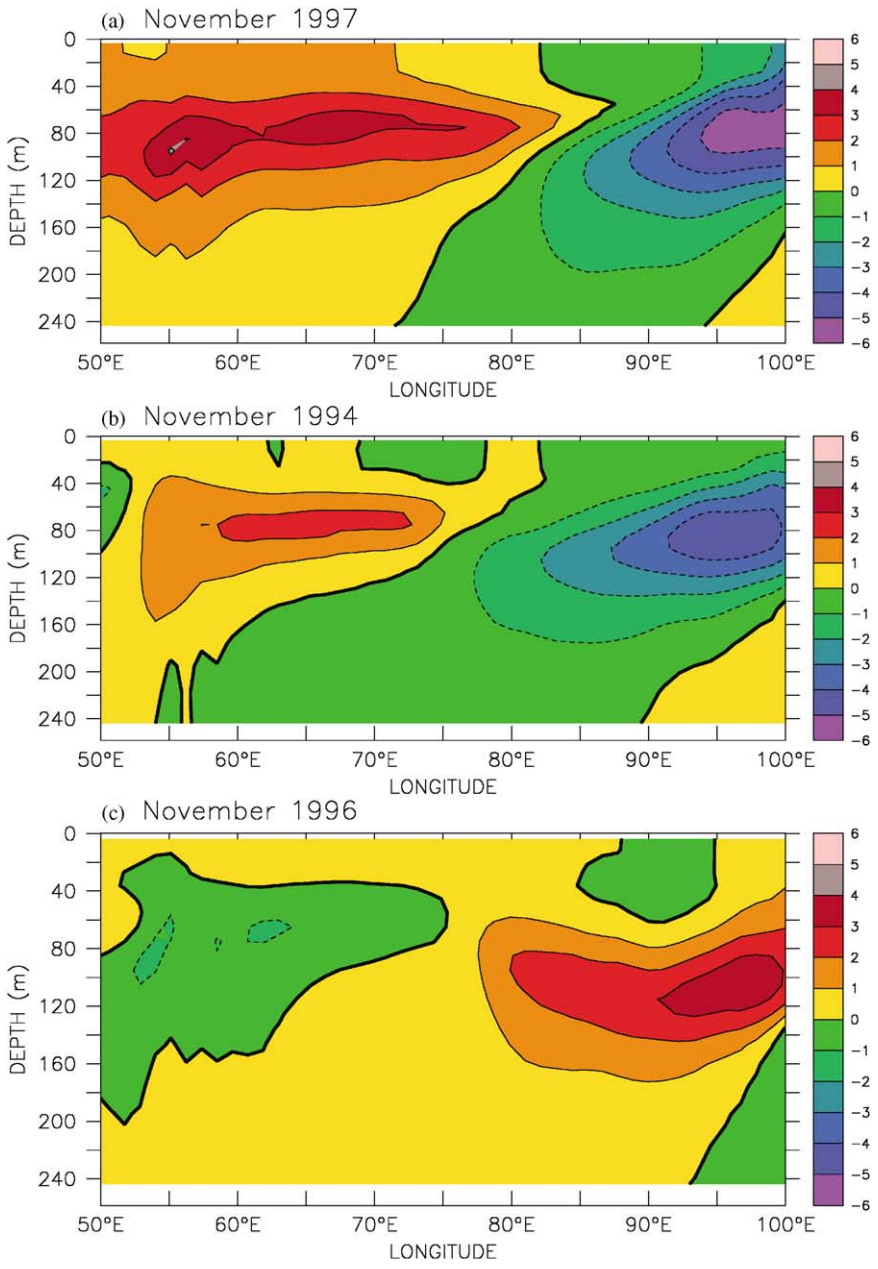


Fig. 8. Subsurface temperature anomaly from the model results during DM events. Temperature anomaly along 5°S is plotted for the upper 250 m. (a) November 1997, (b) November 1994 and (c) November 1996.

in Fig. 11. The positive SSH anomalies correspond to a deeper thermocline in the southwestern Indian Ocean during October–December, 1997 and the negative SSH anomalies correspond to a shallow thermocline off the coast of Sumatra. Comparison of Figs. 9 and 11 reveals that the seasonal evolution of these two parameters is very similar. The upwelling in the model appears to be stronger,

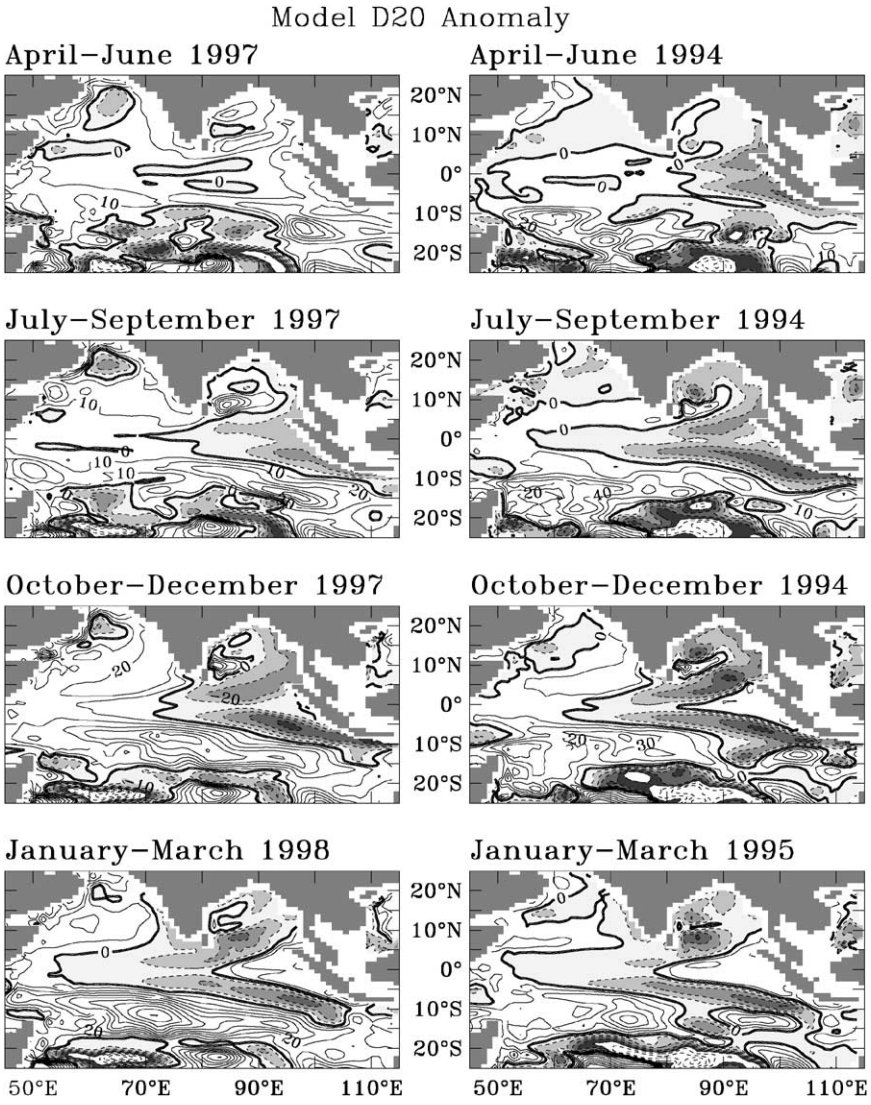


Fig. 9. Seasonal evolution of the anomalies of D20 during the positive DM events of 1997 (left panels) and 1994 (right panels). Contour interval is 10 m. Negative anomalies are shaded.

particularly during 1994 when the negative D20 anomalies stretch farther westward than the SSH anomalies. The negative D20 anomalies are directly related to the negative SSH anomalies and cold SST anomalies. However, the opposite is not true; the deepening of the thermocline and positive SSH anomalies does not necessarily correspond to warm SST anomalies. This is due to the asymmetric effect of upwelling on the SST anomalies. Upwelling brings cold water upwards and cools the sea surface, but a downwelling need not necessarily warm the sea surface (see also Yu and Reinecker, 2000). Therefore, the high in SST and SSH are not always located in the same region.

### 4.2. Negative phase: 1996

The most intense negative DM in the recent decade occurred during 1996 (SGVY, Fig. 2). The

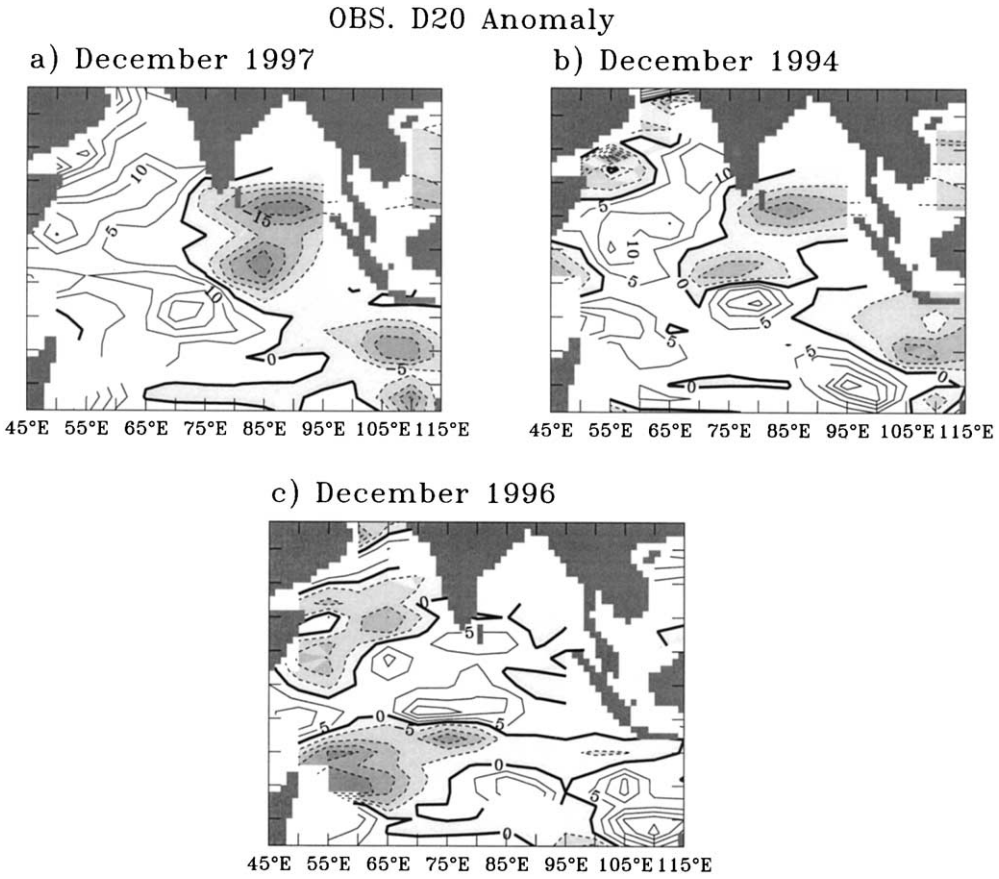


Fig. 10. Observed D20 anomaly during (a) December 1997, (b) December 1994 and (c) December 1996. Contour interval is 5 m. Negative anomalies are shaded.

spatial pattern of the anomalies has their sign opposite to that during a positive DM. The magnitude of the anomalies, however, are weaker during the negative phase and the seasonal evolution less dramatic. The wind anomalies along the equator are westerly during 1996, which appear in spring and stay through fall (Fig. 12). Strong northwesterly wind anomalies are present in the south eastern Indian Ocean during summer, with downwelling favorable along-shore component off Sumatra. The southwest monsoon winds are weak over the Arabian Sea and Bay of Bengal.

Both observations (Fig. 3) and model (Fig. 13) show an east–west contrast in SST with warm anomalies in the east and cold anomalies in the west during summer and fall. The maximum anomalies of 1.0°C appear in the model results during fall at about 10°S in the eastern part of the ocean. The maximum subsurface anomalies exceed 3°C at 100 m in the eastern Indian Ocean and 1°C in the west (Fig. 8).

MLD anomalies are positive corresponding to a deepening of the mixed layer in the east during summer and fall. In the west there is no distinct shallowing of the mixed layer. The D20 (Fig. 14) anomalies show deeper than normal thermocline in the east and shallower thermocline in the west. The deepening begins in spring and peaks during fall. The two highs of positive D20 anomalies located on either side of the equator clearly indicate the presence of a downwelling Rossby wave excited during the negative phase of the DM.

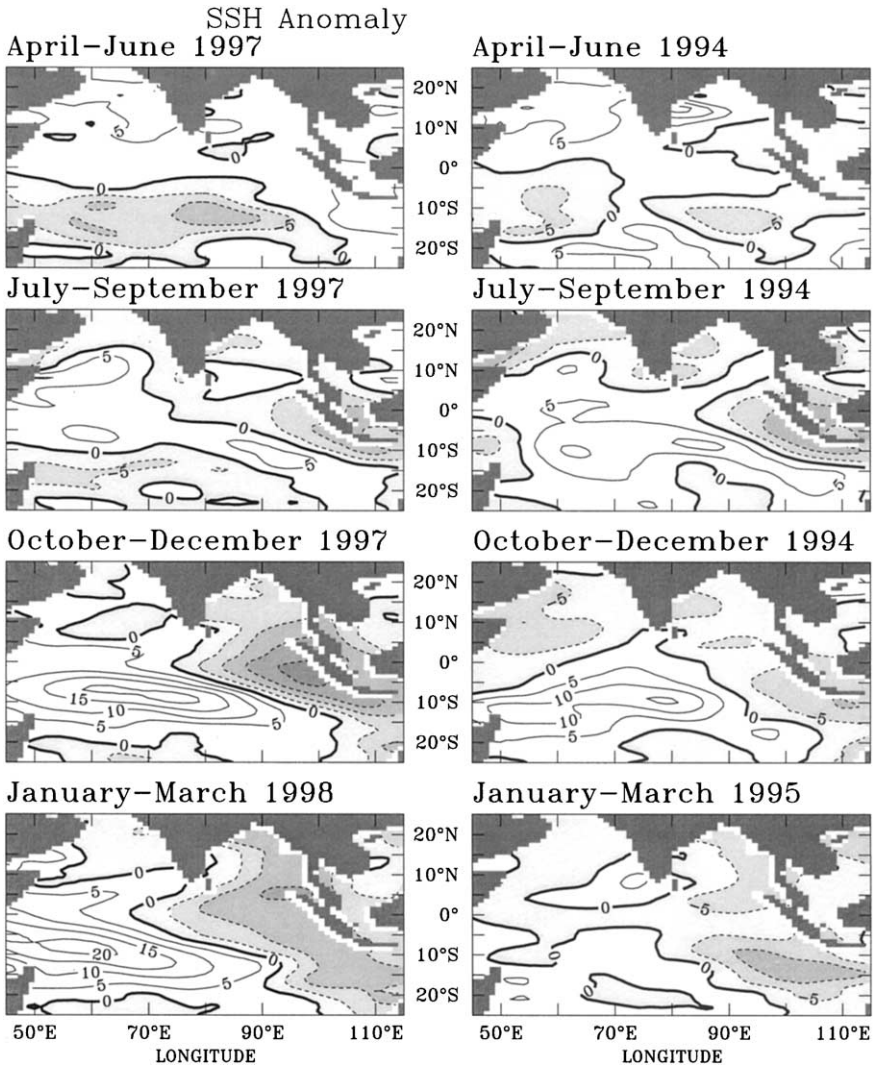


Fig. 11. Seasonal evolution of the SSH anomalies from TOPEX/Poseidon during the positive DM events of 1997 (left panels) and 1994 (right panels). Contour interval is 5 cm. Negative anomalies are shaded.

Observed D20 anomalies are consistent with this model result (Fig. 10, bottom panel), but this Rossby wave is not seen clearly in the SSH anomalies.

### 4.3. Equatorial jets

A spectacular feature of the circulation in the upper equatorial Indian Ocean is the appearance of the eastward equatorial jets during the transition between monsoons (Wyrtki, 1973). Fig. 15a shows the climatology of zonal currents along the equator. The simulated jets are very similar to that inferred from ship drifts (Han et al., 1999). The fall jet, however, is weaker in the model, and this is most probably due to the lack of fresh-water forcing in the model (Han et al., 1999). The jets accumulate water in the eastern Indian Ocean, leading to a warm SST and a deep mixed layer and thermocline (Hastenrath et al., 1993). The wind anomalies along the equatorial Indian Ocean during the DM events affect the jets. Fig. 15b–d

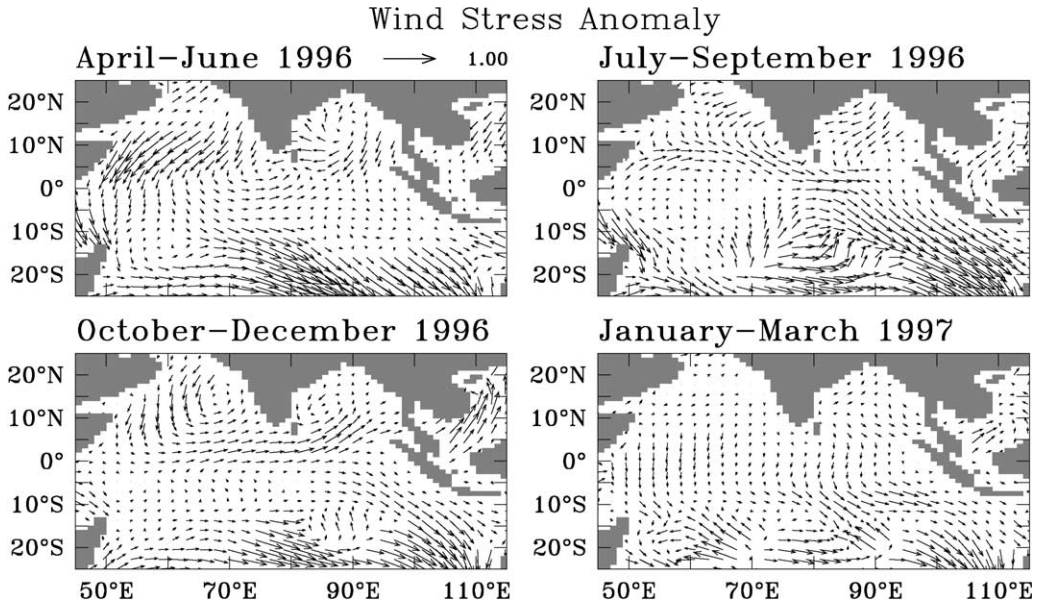


Fig. 12. Seasonal evolution of the anomalies of wind stress (dyne $cm^{-2}$) during the negative DM event of 1996.

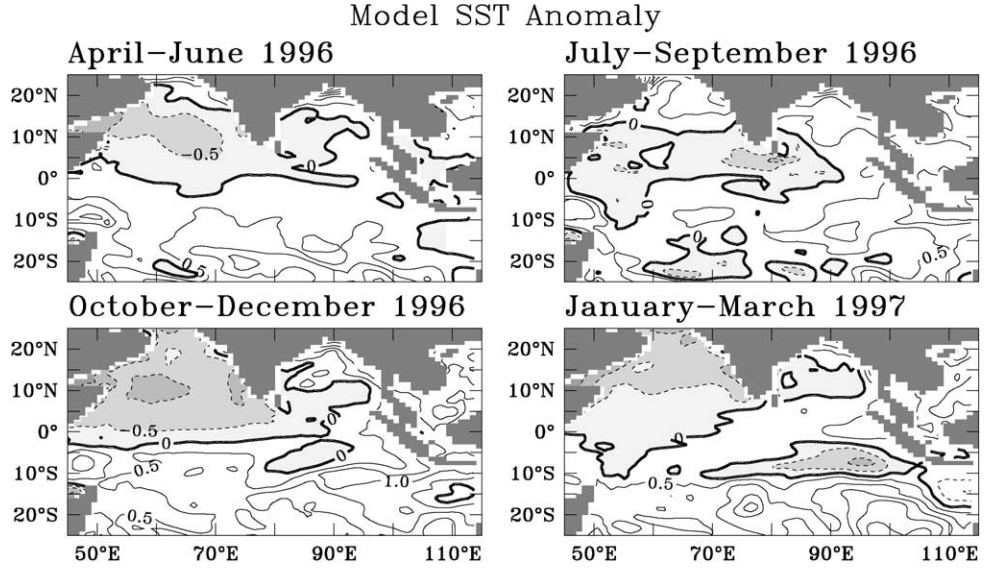


Fig. 13. Seasonal evolution of the anomalies of model SST during the negative DM event of 1996. Contour interval is 0.5°C. Negative anomalies are shaded.

elucidates the effect of equatorial wind anomalies during dipole events on the jets. The jets are weak during positive DM events and strong during negative DM events. The strongest anomaly is seen during 1997 when the anomalous westward winds forced a westward current along the equatorial Indian Ocean (Fig. 15d). During 1994, as a result of the westward wind anomalies, the

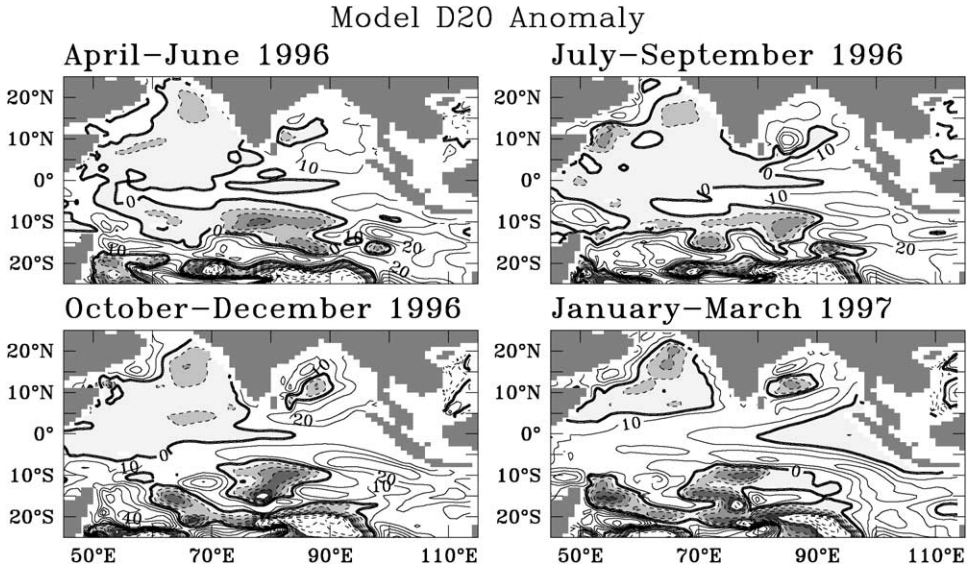


Fig. 14. Seasonal evolution of the anomalies of D20 during the negative DM event of 1996. Contour interval is 10 m. Negative anomalies are shaded.

equatorial jets were very weak (Fig. 15c), and consequently the sea level and SST in the eastern equatorial Indian Ocean remained unusually low (Vinayachandran et al., 1999b). Observations made in the equatorial Indian Ocean during 1994 (Reppin et al., 1999) showed a weak jet during 1994 consistent with the model simulation (Vinayachandran et al., 1999b).

## 5. Heat budget

In order to understand the processes that determine the SST anomalies we calculated the heat budget. In the model the temperature tendency is given by

$$T_t = -(uT_x + vT_y + wT_z) + \frac{Q_s}{\rho C_p h} + D,$$

where $D$ represents the diffusion terms and $Q_s$ is the net surface heat flux. The terms of the above equation for the upper 50 m in the western (50°E–70°E, 5°S–5°N) and eastern (90°E–110°E, 10°S–0°) Indian Ocean along with SST anomalies are shown in Fig. 16. All terms are calculated from the monthly mean model outputs and anomalies with respect to 1975–1998 are shown. It should be noted that the heat flux parameterization in the model (Appendix A) is limited by the use of air temperature and humidity which forces the SST simulations towards observations.

The large cooling in the eastern Indian Ocean during positive DM of 1997 and 1994 (Fig. 16c) is mainly due to upwelling of cold water (Fig. 16d) that takes place off the coast of Sumatra (Fig. 3). The upwelling brings cold water to the surface and this water advects northwestward along the coast of Sumatra and westward along the equator (Fig. 7). During 1994, the upwelling (Fig. 16d) had its maximum intensity during summer and the peak SST anomalies occurred about two months earlier compared to 1997 (Fig. 7). The upwelling during 1994 is overestimated in the model, and this leads to larger SST anomalies in the eastern Indian Ocean than during 1997. Towards the end of the positive DM, downwelling replaces upwelling (Fig. 9) and the eastern Indian Ocean begins to warm primarily due to the surface heat flux (Fig. 16d). The cold SST anomalies and weakening winds (Fig. 6) cause reduction in latent heat loss

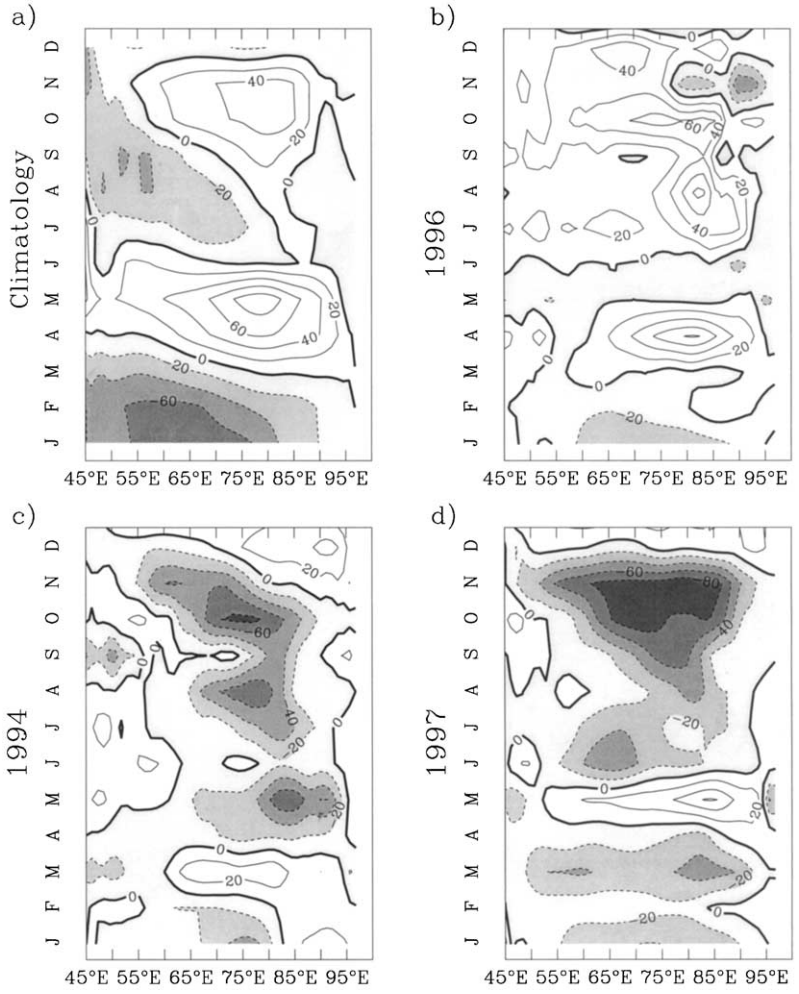


Fig. 15. (a) Climatology of zonal currents (cm $s^{-1}$) along the equator from the model, (b) Anomaly of zonal current from the model during 1996, (c) during 1994 and (d) during 1997.

leading to positive surface heat flux anomaly (Murtugudde et al., 2000). The warming is rapid as the mixed layer is very thin (Fig. 4). The horizontal advection of warmer water from the north (Fig. 7) also appears to contribute to the warming.

The warming in the western Indian Ocean during positive DM of 1997 and 1994 (Fig. 16a) is chiefly due to horizontal advection and downwelling (Fig. 16b). During the summer of 1994, however, an increase in surface heat flux and horizontal advection also contribute towards the warming of the SST anomaly. This is consistent with the MLD anomalies presented in Fig. 4, which suggests that the deep mixed layer in the model during 1997 was caused by ocean dynamics but during 1994 the surface fluxes modulated the mixed layer during summer.

The warming in the east during the negative DM of 1996 is attributed to the surface heat flux. Advection of cooler water from the surroundings (Fig. 13) tend to cool the surface. This water then warms by air-sea fluxes and downwells (Fig. 14) in the region considered here. In the west, cold SST

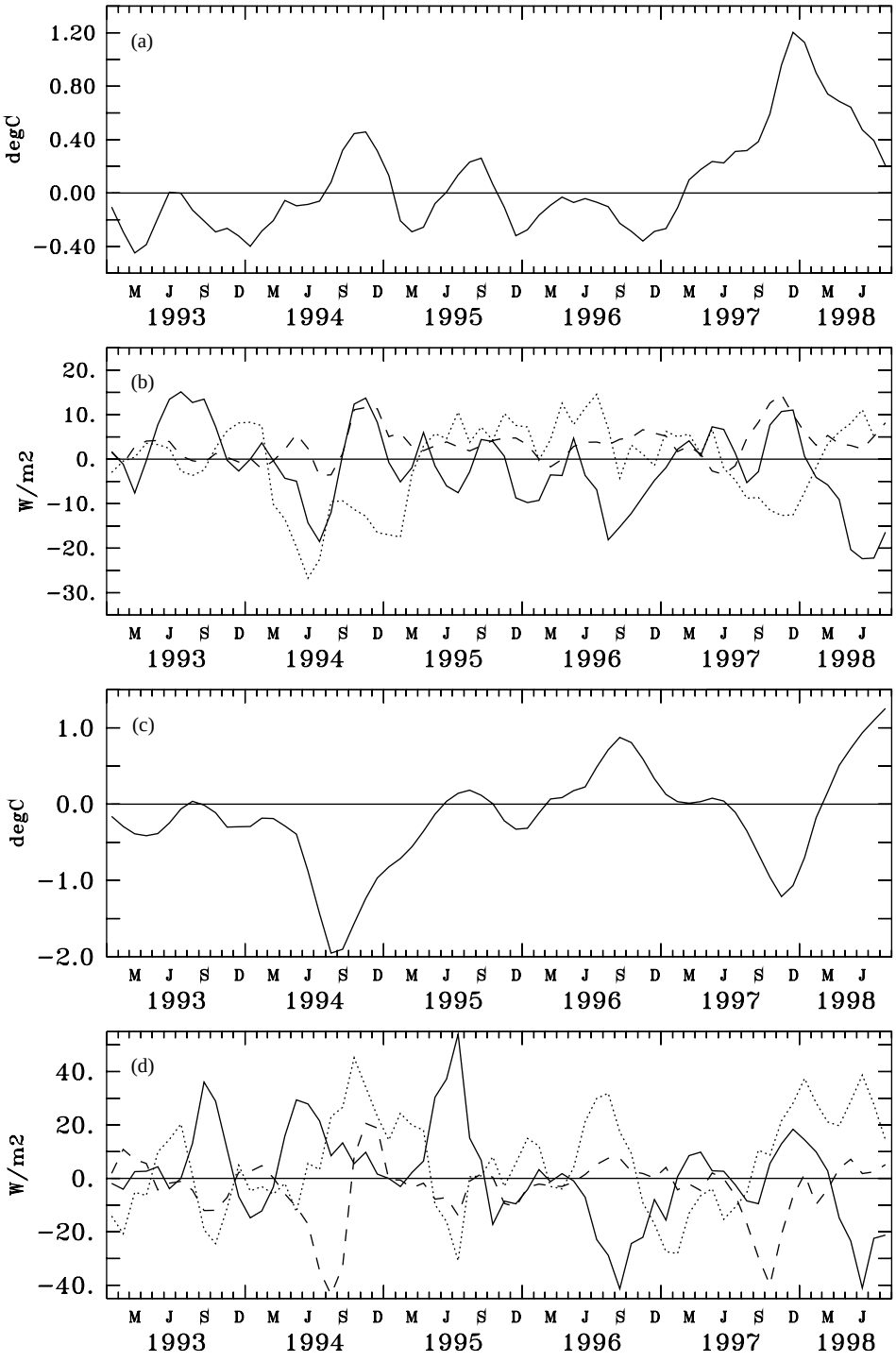


Fig. 16. (a) Model SST anomalies in the western 50°E–70°E, 5°S–5°N) Indian Ocean. (b) Anomalies of net surface heat flux (dotted line) horizontal advection (solid line) and vertical advection (dashed line) in the upper 50 m of the model, in the western Indian Ocean. (c) Same as in (a) but for the eastern (90°E–110°E, 10°S–0°) Indian Ocean. (d) Same as in (b) but for the eastern Indian Ocean.

anomaly is due to the combined effect of $Q_s$ and horizontal advection, with the latter being the major contributor.

The above model results suggest that the cooling of the eastern Indian Ocean during the positive phase of the DM events is governed by oceanic processes namely upwelling and advection. During the negative DM events the warming in the east is attributed to net surface heat flux. In the west, during both phases of the DM the net surface heat flux as well as advection–downwelling determines the SST anomalies albeit their relative contribution vary between seasons and events. Upwelling and downwelling are found to play an important role during both positive events of 1994 and 1997. Therefore, below we examine the role of Rossby wave as a possible mechanism in generating the DM pattern.

## 6. Role of Rossby waves

Kelvin and Rossby waves play an important role on the seasonal dynamics and thermodynamics of the tropical Indian Ocean, particularly in the equatorial and coastal regions (McCreary et al., 1993). Chambers et al. (1999) found that the Rossby wave in the southern tropical Indian ocean caused the warming in the western Indian Ocean during 1994 and 1997. Murtugudde et al. (2000) suggested that the downwelling Rossby wave caused the warming in the western Indian Ocean to sustain until February 1998. The latter two studies suggest that interannual fluctuation of winds in the Indian Ocean can excite Kelvin and Rossby waves that could alter the thermal structure of the Indian Ocean from its normal seasonal pattern. In this section, we examine the role of such waves on the east–west contrast in the thermal structure observed during DM events.

Fig. 17b shows the model D20 anomaly, along the equator, averaged between 5°N–5°S. Similar picture from the observations is also shown (Fig. 14a). The patterns of anomalies are very similar in both panels. Major difference is during 1995–1996, when the model results show mostly positive anomalies and the observations show weak negative anomalies.

During the positive DM events of 1994 and 1997 the easterly wind anomalies along the equator excite an upwelling Kelvin wave along the equator. This Kelvin wave, on reaching the eastern boundary, lifts the thermocline in the eastern equatorial Indian Ocean and reflects as an upwelling Rossby wave which propagates westward (Fig. 17). The upwelling Rossby wave propagates westward moving the cold SST anomalies westward along the equatorial Indian Ocean (Fig. 7). As the wind anomalies relax, the upwelling is replaced by downwelling (Fig. 9, bottom panels), which leads to the decay of the SST anomalies. The collapse of the upwelling gives rise to a downwelling Rossby wave during the year following positive DM (here 1995 and 1998) (Fig. 9 lower panels, Fig. 17).

The positive DM events are preceded by a downwelling Rossby wave that originates from the eastern boundary. One such signal can be seen originating during 1993 and propagating westward and the other during 1996 in both model and data (Fig. 17). The deepening of the thermocline in the west during both 1994 and 1997 can be traced to the downwelling Rossby waves generated during 1993 and 1996, respectively. Possible mechanism that can generate such a Rossby wave is the reflection of a downwelling equatorial Kelvin wave generated by westerly wind anomalies (Fig. 12). This downwelling Rossby wave is significantly amplified in the central Equatorial Ocean as it propagates westward and also its phase speed increases in the central equatorial Indian Ocean, which is indicated by a change in the slope of the contours (Fig. 17).

The meridional symmetry of the D20 anomalies with maximum anomalies at about 5°N (Fig. 9) suggests that these are primarily first baroclinic Rossby waves. Observations (Fig. 10) confirm that this is a real natural process. The slope of the contours suggests that the signal can cross the Indian Ocean in about 12 months, giving a phase speed of about 17 cm $s^{-1}$, which is consistent with theoretical values and that obtained from SSH anomalies (Chambers et al., 1999).

Chambers et al. (1999) and Webster et al. (1999) noted that anomalous Rossby wave in the southern tropical Indian Ocean during 1994 and 1997

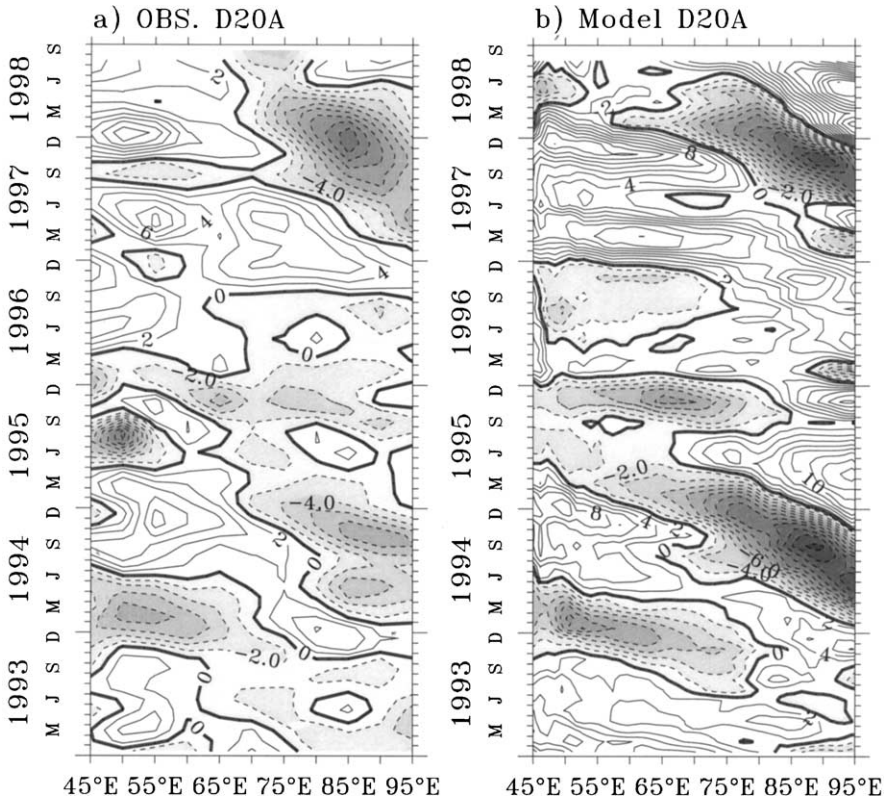


Fig. 17. Time longitude plot of (a) observed (left panel) and modeled (right panel) D20 anomalies averaged between 5°N and 5°S. The anomalies are smoothed by a 3-month running mean before plotting.

played an important role in the warming in those years. The model results also show large positive D20 anomalies consistent with their inference (Fig. 9). Examination of the wind stress curl (Fig. 18) suggests that Ekman pumping was responsible for the generation of this Rossby wave in the model (Masumoto and Meyers, 1998). In order to test this, we examined the role of local Ekman pumping and Rossby wave radiation from the east on the upwelling/downwelling in the model. For this purpose, we present the vertical velocity from the model (full line) at a depth of 50 m for the region 60°E–80°E; 15°S–5°S in Fig. 19. The Ekman pumping and the difference between the two is also shown. The latter is assumed to be due to the Rossby waves propagating from the east. The anomalies with respect to the climatology during 1975–1998 are presented. The dominance of Ekman pumping is clearly seen in the figure. The only exception is during the summer of 1994, when the Rossby wave from the east is larger than the Ekman pumping.

## 7. Summary and conclusions

The positive DM in the Indian Ocean is characterized by cold SST anomalies in the eastern equatorial Indian Ocean and warm SST anomalies in the west. The wind anomalies are easterly along the equator during these events, alongshore off the coast of Sumatra, northwesterly in the southern tropical Indian Ocean, and southwesterly in the Arabian Sea and Bay of Bengal. The thermocline in the eastern Indian Ocean becomes shallower than usual and deeper in the west. This is manifested in the form of a fall in the sea level in the eastern Indian Ocean and a rise in the western

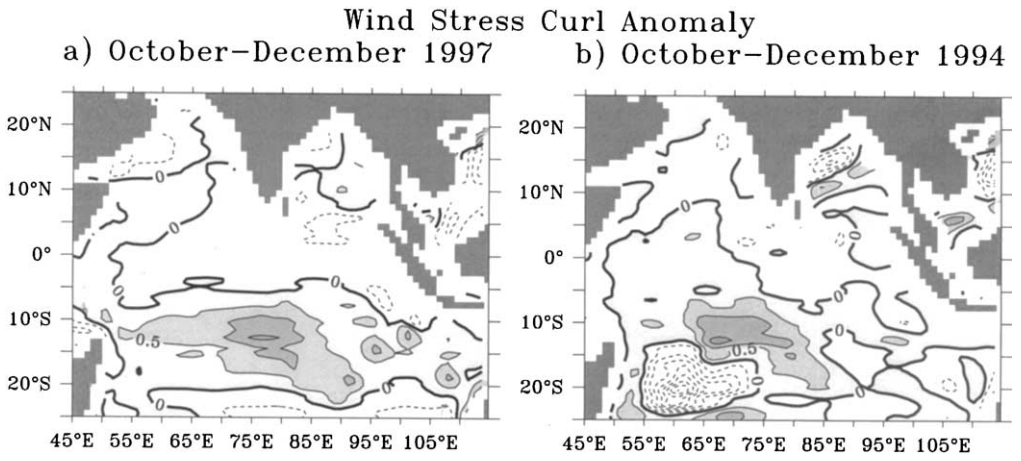


Fig. 18. Wind stress curl anomaly averaged for the period October–December (a) 1997 and (b) 1994. Contour interval is $0.5 \times 10^{-8}$ dyne $cm^{-3}$. Positive values are shaded.

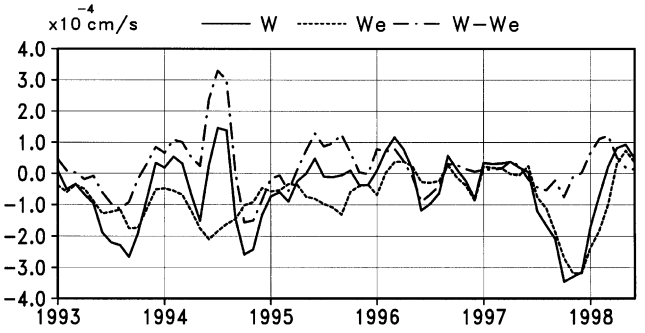


Fig. 19. Vertical velocity at 50 m from the model (solid line), Ekman pumping (dashed line) and the difference between the two (dot–dash line). All quantities are anomalies from the 1975–1998 climatology and average over the region (60°E–80°E, 15°S–5°S).

Indian Ocean. We have simulated the evolution of the dipole mode events using an ocean model forced by NCEP fluxes for the period 1975–1998. Both observations and model indicate a negative DM during 1996, with the anomalies exhibiting a pattern opposite to that during the positive phase, though less dramatic and weak. The model captures all the observed events, and the patterns of anomalies are reasonably well reproduced by the model. However, the simulations are limited by the inaccuracies in the surface fluxes in the western Indian Ocean and overestimation of upwelling.

The model results suggest that Kelvin and Rossby wave propagation plays an important role during the DM events. The wind anomalies excite equatorial Kelvin waves, which reflect from the eastern boundary as long Rossby waves that propagate westward. The easterly wind anomalies during 1994 and 1997 (Murtugudde et al., 2000) excited an upwelling Kelvin wave in the equatorial Indian Ocean. This Kelvin wave reflected primarily as a first baroclinic mode upwelling Rossby wave. The enhanced cooling in the east is caused by coastal upwelling that took place over a mixed layer that was shallower than usual, causing the SST anomalies to be maximum south of the equator off Sumatra. Heat budget based on the model temperature equation confirm this: the

cooling of the eastern Indian Ocean during positive DM events is caused by upwelling and the subsequent warming by surface heat flux. The cold SST anomalies in the eastern Indian Ocean decay after the Rossby wave departs and the upwelling is replaced by downwelling.

A downwelling Rossby wave excited during the negative DM event of 1996 played a crucial part in causing the anomalously deep thermocline in the western equatorial Indian Ocean during early 1997. A similar process happened during 1993–1994 as well. The model heat budget, although somewhat limited by poor mixed-layer simulation in the western Indian Ocean, confirms the role of ocean dynamics during the positive DM events. The reduced latent heat flux (Yu and Reinecker, 2000) caused warm SST anomalies in the southern tropical Indian Ocean during 1997. A long Rossby wave excited by the anomalous Ekman pumping contributed to this warming in our model (Chambers et al., 1999).

Our knowledge of the climate events in the Pacific has progressed much farther than that of the Indian Ocean because of the introduction of an observational network during the TOGA period (McPhaden et al., 1998). The revelation of the DM event has been possible mainly due to surface observations, satellite data, and a few subsurface observations. Detailed information is still lacking. For example, observations needed to trace the path of the Rossby waves are sparse. Further, salinity effects are quite important in the equatorial Indian Ocean (Vinayachandran et al., 1999a; Han et al., 1999) and no known measurement of subsurface salinity exist in the Indian Ocean during the last two strong DM events. It is important that an observational network be installed in the Indian Ocean so that evolution of climate events such as DM can be monitored, understood and can be used for predicting disastrous climate events at least in the surrounding countries.

## Acknowledgements

This study was possible because of the availability of several data sets through the internet. The TOPEX/Poseidon data were obtained from www.csr.utexas.edu (thanks to Dr. D.P. Chambers) and gridded subsurface temperature data from jedac.ucsd.edu (thanks to Dr. Warren B. White). We thank Ron Pacanowski for providing the original MOM2.2 code. Graphics were generated using FERRET. We also thank Dr. Sha Ping Xie and an anonymous reviewer for their constructive comments and suggestion on the manuscript. This work was partially supported by FRSGC of JAMSTEC/NASDA as well as the Japan Science and Technology Agency through the NIED. PNV was partially supported by the start-up grant of the Indian Institute of Science and the INDOMOD program of the Department of Ocean Development, Government of India.

## Appendix A. Formulation of surfaces fluxes in the model

The surface heat flux $Q$ is calculated using the formula

$$Q = Q_{\mathrm{sw}}\downarrow - Q_{\mathrm{sw}}\uparrow + Q_{\mathrm{lw}}\downarrow - Q_{\mathrm{lw}}\uparrow - Q_{\mathrm{sensible}} - Q_{\mathrm{latent}},$$

where $Q_{\mathrm{sw}}\downarrow$, $Q_{\mathrm{sw}}\uparrow$, $Q_{\mathrm{lw}}\downarrow$, $Q_{\mathrm{lw}}\uparrow$, $Q_{\mathrm{sensible}}$, and $Q_{\mathrm{latent}}$ are surface downward and upward short wave radiation, surface downward and upward longwave radiation, sensible heat flux, and latent heat flux, respectively. $Q_{\mathrm{sw}}\downarrow$, $Q_{\mathrm{sw}}\uparrow$, and $Q_{\mathrm{lw}}\downarrow$ are derived from NCEP/NCAR reanalysis data (Kalnay et al., 1996). Upward longwave radiation is computed as

$$Q_{\mathrm{lw}}\uparrow = \sigma T_{\mathrm{sst}}^4,$$

where $\sigma$ is Stefan–Boltzmann constant and $T_{\mathrm{sst}}$ is the model SST. The sensible and latent heat fluxes are estimated by

$$Q_{\mathrm{sensible}} = \rho_{\mathrm{a}} C_{\mathrm{p}} C_{\mathrm{h}} |\mathbf{V}|(\mathbf{T}_{\mathrm{a}} - \mathbf{T}_{\mathrm{sst}}),$$
$$Q_{\mathrm{latent}} = \rho_{\mathrm{a}} L C_{\mathrm{h}} |\mathbf{V}|(\mathbf{q}_{\mathrm{a}} - \mathbf{q}_{\mathrm{sst}}),$$

where $\rho_{\mathrm{a}}$ is air density, $\mathbf{V}$ is wind speed at 10 m, $T_{\mathrm{a}}$ is surface air temperature, $q_{\mathrm{a}}$ is surface air humidity, and $q_{\mathrm{sst}}$ is saturation humidity at the model SST.

Similarly, the surface zonal and meridional momentum fluxes are given by

$$\tau^x = \rho_a C_m |\mathbf{V}| \mathbf{u}_{10\,m},$$
$$\tau^y = \rho_a C_m |\mathbf{V}| \mathbf{v}_{10\,m},$$

where $u_{10\,m}$ and $v_{10\,m}$ are the zonal and meridional components of the winds at a height of 10 m, respectively. The drag coefficient $C_h$ and $C_m$ are estimated according to the similarity function proposed by Louis et al. (1982).

## References


Behera, S.K., Krishnan, S., Yamagata, T., 1999. Unusual ocean–atmosphere conditions in the tropical Indian Ocean during 1994. Geophysical Research Letters 26, 3001–3004.

Chambers, D.P., Tapley, B.D., Stewart, R.H., 1997. Long-period ocean heat storage rates and basin-scale heat fluxes from TOPEX. Journal of Geophysical Research 102, 10525–10533.

Chambers, D.P., Tapley, B.D., Stewart, R.H., 1999. Anomalous warming in the Indian Ocean coincident with El Niño. Journal of Geophysical Research 104, 3035–3047.

Dukowicz, J.K., Smith, R.D., 1994. Implicit free-surface method for the Bryan–Cox–Semtner ocean model. Journal of Geophysical Research 99, 7991–8014.

Han, W., McCreary, J.P., Anderson, D.L.T., Mariano, A.J., 1999. On the dynamics of the eastward surface jets in the equatorial Indian Ocean. Journal of Physical Oceanography 29, 2191–2209.

Hastenrath, S., Nicklis, A., Greischar, L., 1993. Atmospheric–hydrospheric mechanisms of climate anomalies in the western equatorial Indian Ocean. Journal of Geophysical Research 98, 20219–20235.

Hellerman, S., Rosenstein, M., 1983. Normal monthly wind stress over the world ocean with error estimates. Journal of Physical Oceanography 13, 1093–1104.

Iizuka, S., Matsuura, T., Yamagata, T., 2000. The Indian Ocean SST dipole simulated in a coupled general circulation model. Geophysical Research Letters 27, 3369–3372.

Kalnay, E., Kanamitsu, M., Kistler, R., Collins, W., Deaven, D., Gandin, L., Iredell, M., Saha, S., White, G., Woolen, J., Zhu, Y., Chelliah, M., Ebisuzaki, W., Higgins, W., Janowiak, J., Mo, K.C., Ropelewski, C., Wang, J., Leetma, A., Reynolds, R., Jenne, R., Joseph, D., 1996. The NCEP/NCAR 40 years reanalysis project. Bulletin of American Meteorological Society 77, 437–471.

Kawamura, R., Matsuura, T., Iizuka, S., 2001. Role of an equatorially asymmetric mode in the Indian Ocean in the Asian summer monsoon-ENSO coupling. Journal of Geophysical Research 106, 4681–4693.

Levitus, S., 1982. Climatological Atlas of the World Ocean. NOAA professional paper no. 13, U.S. Govt. Printing Office, Washington, D.C., 173pp.

Louis, J., Tiedtke, M., Geleyn, J.F., 1982. A short history of PBL parameterization at ECMWF. Workshop on Planetary Boundary Layer Parameterization, ECMWF, pp. 59–80.

Marotzke, J., 1991. Influence of convective adjustment on the stability of the thermohaline circulation. Journal of Physical Oceanography 21, 903–907.

Masumoto, Y., Meyers, G., 1998. Forced Rossby waves in the southern tropical Indian Ocean. Journal of Geophysical Research 103, 27589–27602.

Matsuura, T., Yumoto, M., Iizuka, S., Kawamura, R., 1999. Typhoon and ENSO simulation using a high-resolution coupled GCM. Geophysical Research Letters 26, 1755–1758.

McCreary, J.P., Kundu, P.K., Molinari, R., 1993. A numerical investigation of the dynamics, thermodynamics and mixed layer processes in the Indian Ocean. Progress in Oceanography 31, 181–244.

McPhaden, M.J., Busalacchi, A.J., Cheney, R., Donguy, J.R., Gage, K.S., Halpern, D., Ji, M., Julian, P., Meyers, G., Mitchum, G.T., Niiler, P.P., Picaut, J., Reynolds, R.W., Smith, N., Takeuchi, K., 1998. The tropical ocean–global atmosphere observing system: a decade of progress. Journal of Geophysical Research 103, 14169–14240.

Meyers, G., Pigot, L., 2000. Analysis of frequently repeated XBT lines in the Indian Ocean. CSIRO Marine Laboratories Report 238, 43pp.

Murtugudde, R., Signorini, S.R., Christian, J.R., Busalacchi, A.J., McClain, C.R., Picaut, J., 1999. Ocean color variability of the tropical Indo-Pacific basin observed by SeaWIFS during 1997–1998. Journal of Geophysical Research 104, 18351–18366.

Murtugudde, R., McCreary, J.P., Busalacchi, A., 2000. Oceanic processes associated with anomalous events in the Indian Ocean with relevance to 1997–1998. Journal of Geophysical Research 105, 3295–3306.

Pacanowski, R.C., 1996. Documentation, users guide, and reference manual (MOM2, Version 2). GFDL Technical Report 3.2, 329pp.

Pacanowski, R.C., Philander, S.G.H., 1981. Parameterization of vertical mixing in numerical models of tropical oceans. Journal of Physical Oceanography 111, 1443–1451.

Paulson, C.A., Simpson, J.J., 1977. Irradiance measurements in the upper ocean. Journal of Physical Oceanography 7, 952–956.

Philander, S.G.H., 1990. El Niño, La Niña and the Southern Oscillation. Academic Press, New York, 289pp.

Rayner, N.A., Horton, E.B., Parker, D.E., Folland, C.K., Hackett, R.B., 1996. Version 2.2 of the Global Sea Ice Sea Surface Temperature Data Set. Clim. Res. Tech. Note. 74, UK Meterological Office, Bracknell.

Reppin, J., Schott, F., Fischer, J., Quadfasel, D., 1999. Equatorial currents and transports in the Indian Ocean: annual cycle and interannual variability. Journal of Geophysical Research 104, 15495–15514.

Saji, N.H., Goswami, B.N., Vinayachandran, P.N., Yamagata, T., 1999. A dipole mode in the tropical Indian Ocean. Nature 401, 360–363.

Tapley, B.D., Chambers, D.P., Shum, C.K., Eanes, R.J., Ries, J.C., Stewart, R.H., 1994. Accuracy assessment of the large-scale dynamic ocean topography from TOPEX/Poseidon altimetry. Journal of Geophysical Research 99, 24605–24617.

Tourre, Y.M., White, W.B., 1997. Evolution of ENSO signals over the Indo-Pacific domain. Journal of Physical Oceanography 27, 683–696.

Vinayachandran, P.N., Masumoto, Y., Mikawa, T., Yamagata, T., 1999a. Intrusion of the southwest monsoon current into the Bay of Bengal. Journal of Geophysical Research 104, 11077–11085.

Vinayachandran, P.N., Saji, N.H., Yamagata, T., 1999b. Response of the equatorial Indian Ocean to an unusual wind event during 1994. Geophysical Research Letters 26, 1613–1615.

Webster, P.J., Moore, A.M., Loschnigg, J.P., Leben, R.R., 1999. Coupled ocean–atmosphere dynamics in the Indian Ocean during 1997–1998. Nature 401, 356–360.

White, W.B., Pazan, S.E., Withee, G.W., Noe, C., 1988. Joint Environmental Data Analysis (JEDA) Center for scientific quality control of upper ocean thermal data in support of TOGA and WOCE. EOS Transactions, American Geophysical Union 69, 122–123.

Wyrtki, K., 1973. An equatorial jet in the Indian Ocean. Science 181, 262–264.

Yu, L., Reinecker, M.M., 1999. Mechanisms for the Indian Ocean warming during 1997–1998 El Niño. Geophysical Research Letters 26, 735–738.

Yu, L., Reinecker, M.M., 2000. Indian Ocean warming of 1997–1998. Journal of Geophysical Research 105, 16923–16939.